Błażej TORZYK, Bogusław WIĘCEK
LODZ UNIVERSITY OF TECHNOLOGY, INSTITUTE OF ELECTRONICS, 211/215 Wólczańska St., 90-924 Łódź, Poland

Thermal modeling and RMS current measurement in electrical power lines using IR thermography

Abstract

Thermal modeling in frequency domain and experiments using IR thermography are performed to evaluate RMS current in electrical power lines. The model implements interface thermal resistance between the metal core and insulation layer. This allowed matching the results of simulations and measurements with acceptable accuracy. The proposed method requires the use of known values of heat transfer coefficient and thermal parameters of the cable and its insulation. In consequence the proposed method requires calibration.

Keywords: RMS electrical current measurement, heat transfer modeling, overhead power lines, IR thermography.

1. Introduction

The RMS value of AC current is one of the main parameter of electrical power lines [1, 2, 3, 6, 8]. There are various methods to measure this current. The first one used shunts to measure voltage over a small electrical resistance. It was a problem for higher frequency harmonics due to the inductive reactance of such shunts [21]. Current transformers are currently the most used for current measurement. They are mounted in transformer or distribution stations allowing permanent monitoring and measurement [15]. There are popular electrical current sensors operating on Hall-effect principles [22, 23, 24]. Nowadays, optical fibers are used for both power line current and temperature measurements [16]. At present, IR thermography becomes more useful in electrical energy systems as a contactless method allowing monitoring systems during normal operation, sometimes in high voltage conditions [18, 19, 20]. Today, IR thermography is mainly used to locate faults and damages [17]. In addition, there are applications of IR cameras to maintain electrical systems running continuously, and to predict possible abrupt damages [17].

The purpose of this article is an application of IR thermography to estimate the value of the RMS current by measuring mean temperature of a cable with and without insulation. In order to use IR thermography for power lines, the thermal resistance of a cable has to be determined [4, 5, 7, 9, 10].

2. 2D thermal model of insulated electrical cable with an interface thermal resistance

An electrical cable can be modeled as an infinite cylinder made of metallic conductor, with or without insulation. In this work two steel cables were modeled as it is shown in Fig. 1. Radius of the steel cable is R_1, while the outer radius of the insulation layer is R_2.

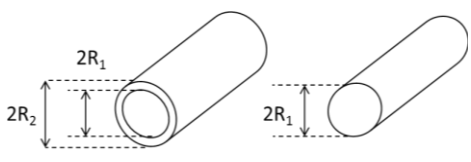

Fig. 1. Two modeled cables with and without insulation

The insulation covers the metal conductor. At first, the heat transfer model assumed an ideal thermal contact between metal and insulation material. In this case, temperature measurements at the outer surface of insulation could not match the simulation results. In consequence, an additional interface thermal resistance R_{thi} between metal and polyvinyl insulation layer was introduced – Fig. 2. For each cable, the value of R_{thi} has to be chosen properly to achieve agreement between simulation and measurement results [8, 13].

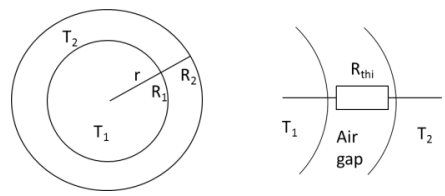

Fig. 2. A cable with insulation separated by an air gap (thermal interface resistance R_{thi})

The heat transfer model used in this work is defined in the frequency domain using Laplace transform. In steel electrical conductor for $r \le R_1$, where the power is dissipated, the Fourier-Kirchhoff equation can be expressed as [11, 18, 19]:

$$k_1 \nabla^2 T_1(r) - j\omega C_{th1} T(r) = -p_v \tag{1}$$

where: p_v – power density, k_1 – thermal conductivity of steel, $C_{th1} - \rho c$ thermal capacity of the cable, ρ - density, c specific heat and ω – angular frequency [4].

For insulation layer, where no power is dissipated, $R_1 < r \le R_2$, the heat conduction equation takes a form:

$$k_2 \nabla^2 T_2(r) - j\omega C_{th2} T(r) = 0 \tag{2}$$

where k_2 and C_{th2} are thermal conductivity and thermal capacity of insulation material, respectively.

Due to the cylindrical symmetry, 3D heat transfer model is reduced and presented by 1D eqs. (3), (5).

For $0 < r \le R_1$

$$k_1 \left(\frac{\partial^2 T_1(r)}{\partial r^2} + \frac{1}{r} \frac{\partial T_1}{\partial r} \right) - j\omega C_{th1} T_1(r) = -p_v \tag{3}$$

For $R_1 < r \le R_2$

$$k_2 \left(\frac{\partial^2 T_2(r)}{\partial r^2} + \frac{1}{r} \frac{\partial T_2}{\partial r} \right) - j\omega C_{th2} T_2(r) = 0 \tag{4}$$

Partial differential equations (3) and (4) have their analytical solutions in the following forms:

$$T_1(r) = A I_0(b_1 r) + \frac{p_v}{j\omega C_{th1}} \tag{5}$$

$$T_2(r) = B I_0(b_2 r) + C K_0(b_2 r) \tag{6}$$

where: A, B, C are the integration constants, I_0, K_0 are the modified Bessel functions of zero order and the parameter $b = \sqrt{j\omega C_{th}/k}$.

The integration constants are calculated using boundary and interface conditions. Typically, it is assumed the continuity of temperature and heat flux at the boundaries and interfaces. However, at the interface between metal cable and polyvinyl insulation, the additional thermal resistance R_{thi} causes the temperature discontinuity.

$$T_1(r)|_{r=R_1} = T_2(r)|_{r=R_1} + R_{thi} P \tag{7}$$

where P is the power transferred from the cable of length L through insulation material to ambient.

$$P = -k_1 \frac{\partial T_1}{\partial r}\Big|_{r=R_1} 2\pi R_1 L \quad (8)$$

Heat flux continuity conditions are established for the interface between the layers and the outer surface, where the convection and radiation cooling transfers thermal energy to ambient [12, 13, 14].

$$-\mathrm{k}_1 \frac{\partial \mathrm{T}_1}{\partial \mathrm{r}}\Big|_{\mathrm{r=R_1}} = -\mathrm{k}_2 \frac{\partial \mathrm{T}_2}{\partial \mathrm{r}}\Big|_{\mathrm{r=R_1}} \quad (9)$$

$$-k_2 \frac{\partial T_2}{\partial r}\Big|_{r=R_2} = hT(R_2) \quad (10)$$

The simulations were performed for the parameters of the cable and environment as close as it was in the experiment [8, 9, 12]. They are listed in Table 1.

Tab. 1. Values of parameters of the thermal model chosen for the simulation

Metal core	Polyvinyl insulation
k_1 = 54 W/mK	k_2 = 0.5 W/mK
ρ_1 = 7800 kg/m^3	ρ_2 = 1300 kg/m^3
c_1 = 490 J/kgK	c_2 = 800 J/kgK
ρ = 1.43·10^{-7} Ωm	-
R_1 = 0.00065 m	R_2 = 0.0014 m
h = 9.5 W/m^{2}K, R_{thi} = 2.3 K/W L = 1 m	

The results of simulation are shown in Figs. 3, 4 and 5, as well as in Table 2. Fig. 3 presents thermal impedance in the form of the Nyquist plots for 2 surfaces of the multilayer structure of the cable: on the insulation and in the metal core. As temperature in the core is almost constant, there is no significant difference between thermal impedances for different positions in the metal conductor. One should notice that thermal impedance is expressed as $Z(j\omega) = T(j\omega)/P$, where P is the Dirac impulse with the amplitude $P = I^2_{RMS} * \rho L/\pi R_1^2$. Power P dissipated in the cable, thermal impedance and resistance vary with its length L. In consequence, temperature does not depend on the cable length and for practical reasons it is worth to evaluate the thermal impedance and resistance per meter length [9, 10].

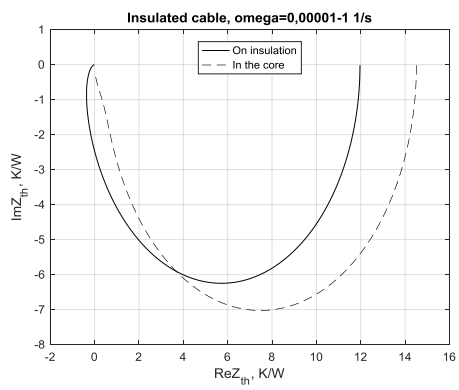

Fig. 3. Nyquist plots of thermal impedance for electrically insulated cable on the insulation and for the point between the core and insulation layers, I_{RMS} = 4,6 A, L = 1 m

In the simulation presented in this paper, one estimated the thermal resistance as the thermal impedance for $\omega \to 0$, $R_{th} = Z_{th}(j\omega \to 0)$. As the Nyquist plot approaches vertically Ox axis for low values of angular frequency (Fig. 3), practically one can assume that $R_{th} \approx \mathrm{abs}\{Z_{th}(\omega < 0.00001)\}$.

In Table 2, simulated temperature for core and insulation is presented. In fact, it is temperature surplus over the ambient one. Both temperature and temperature difference between core and insulation agree with the measured values at the acceptable accuracy (Table 2 and 3).

Tab. 2. Simulated temperature for the cables with and without insulation for different current RMS values (ambient temperature T_a=20.5°C)

I_{RMS}	$T_{insulation}$	T_{core}	ΔT
4.6 A	39.48°C	43.53°C	4.06°C
5.6 A	48.67°C	54.68°C	6.01°C
6.7 A	60.87°C	69.48°C	8.60°C

Finally, the importance of the interface thermal resistance R_{thi} was reported. It was impossible to fit the simulation and measurement temperature with R_{thi} =0. It means that the electrical insulation were not tightly put on steel core of cable. It was made intentionally in order to model the more general thermal configuration with a small air gap between the metal core and polyvinyl insulation layer. Such air gap can appear due to the aging or thermal cycling especially in overhead cables.

In order to compare the cable with and without air gap and different values of interface thermal resistance, 2 simulations were performed for R_{thi}=2.3 K/W and R_{thi}=0 K/W for 1 m length cable. The temperature distributions along radius of the cable for both cases are shown in Figs. 4 and 5. As expected the large discontinuity is observed for a cable with an air gap and non-zero interface thermal resistance both in the model and measurements.

As it can be noticed, the significant temperature drop is on the interface or on the insulation layer. For non-zero thermal interface resistance the discontinuity of temperature at the junction between metal core and insulation layers is observed.

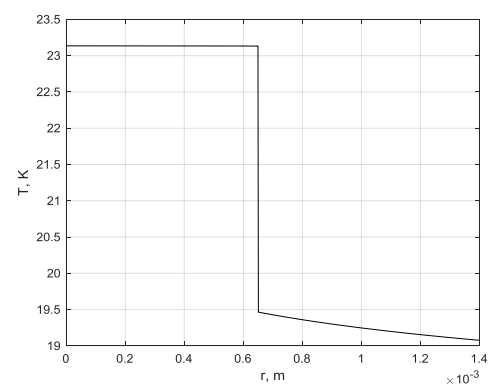

Fig. 4. Temperature difference T_{core}-T_a versus position along the cable radius r for electrically insulated cable with thermal interface resistance R_{thi}=2.3 K/W for L = 1 m, I_{RMS} = 4,6 A

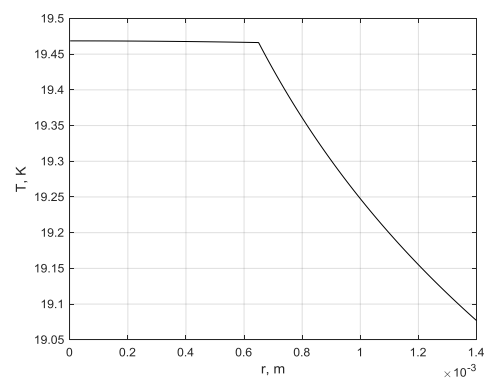

Fig. 5. Temperature versus position along the cable radius r for electrically insulated cable without thermal interface resistance R_{thi}= 0 K/W for L = 1 m, I_{RMS} = 4,6 A

3. Experimental measurements

The procedure of RMS current evaluation using IR thermography is based on measuring temperature of electric cables and thermal modeling to get temperature of the heat source (metal

core). The thermal interface resistance is a novel element of the model which allows matching the simulation and measurement results much easier with better accuracy. The core temperature corresponds directly to the power dissipated in the cable, and in consequence to RMS value of current. The proposed method needs to be calibrated, because temperature depends not only on current, but on the insulation and cooling by convection and radiation, as well. In this work, one assumed that the heat transfer coefficient is known as well as the thermal parameters of the cable and its insulation. The overall proposed procedure is shown in Fig. 6.

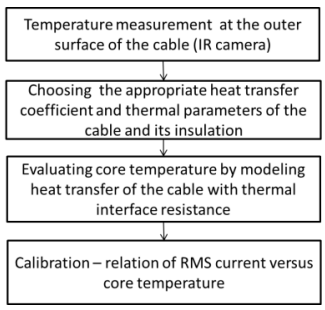

Fig. 6. Proposed procedure of measuring RMS current using temperature measurement by IR camera

All the experiments to verify the method was performed in the laboratory. The cable was connected to the transformer delivering the appropriate power to heat up the element up to 50°C above the ambient temperature in the conditions of natural convection and radiation. In order to verify the model, the cable was partly with and without insulation – Fig. 7. Exemplary thermal image is presented in Fig. 7.

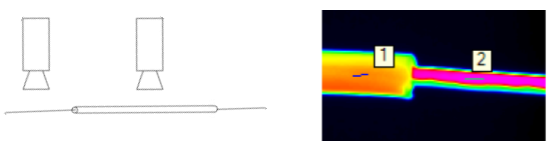

Fig. 7. Experimental setup and exemplary thermal image for estimating RMS current in the electric cable with insulation

4. Results

Thermal images generated by an IR camera were registered and analyzed to determine the mean temperature of a cable with and without insulation for different RMS values of current. The results are presented in Table 3. It can be noticed that the PVC insulation lowers temperature in each of the investigated case by a few degree C in comparison to the cable's core temperature. As expected, the difference of temperature ΔT between the cable's core and ambient temperature rises with increasing current. The expected linear dependence between ΔT and square of RMS current was obtained – Fig. 6.

Temperature calculated using the proposed model shown in Table 2 is very close to the results of the measurement presented in Table 3. It confirms the theoretical assumption of the correlation between temperature changes and RMS current values.

Fig. 8 shows characteristics of temperature changes and RMS current flowing in the cable. This line is practically straight and starts almost from the point (0,0).

The collected data is burdened with errors resulting from the precision of the measuring apparatus and statistical nature of the measurement. On the basis of the following relationships, the uncertainties of average temperature and measured RMS current values were determined [16]. The combined standard uncertainty depends on A and B-type uncertainties and is given as:

$$u_T = \sqrt{u_A^2 + u_B^2} \tag{11}$$

Tab. 3. Temperature measured by IR camera for the cable with and without insulation for different current RMS values

Insulation	Core	Insulation	Core	Insulation	Core
I_{RMS} = 4,6 A		I_{RMS} = 5,6 A		I_{RMS} = 6,7 A	
38.65°C	42.49°C	48.45°C	54.87°C	60.57°C	69.00°C
39.38°C	43.44°C	48.37°C	54.76°C	60.60°C	68.86°C
38.96°C	43.05°C	48.75°C	55.20°C	60.47°C	68.81°C
39.43°C	43.50°C	48.66°C	55.06°C	60.92°C	69.34°C
Mean 39.11°C	Mean 43.12°C	Mean 48.56°C	Mean 54.97°C	Mean 60.64°C	Mean 69.00°C
ΔT =4.02°C		ΔT =6.42°C		ΔT =8.36°C	
$\Delta T/T$ =9.31%		$\Delta T/T$ =11.70%		$\Delta T/T$ =12.12%	

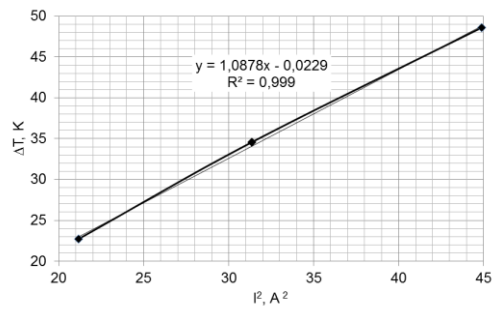

Fig. 8. Measured core temperature surplus over the ambient temperature for the insulated cable

The measurement uncertainty was determined based on the expanded uncertainty U_T.

$$U_T = k_p u_T \tag{12}$$

In this research, the temperature was averaged using 2248 samples extracted from a large sequence of recorded images. All the calculations were made for the core temperature and cable insulation taking N=20 averaged measurement of temperature with 2248 samples each. For such number of measurements the expansion factor k_p=2.13 [16] .

A-type uncertainty for the averaged measurements can be expressed as:

$$u_A = S_{\bar{T}} = \sqrt{\frac{\sum_{i=1}^{N}(T_i - \bar{T})^2}{N(N-1)}} \tag{13}$$

The maximum error of an IR camera used to measure temperature is Δ_{Tg}=2%R, where R is the camera range of measurement. It leads to the B-type uncertainty u_B.

$$u_B = \frac{\Delta_{Tg}}{\sqrt{3}} \tag{14}$$

Table 4 presents the values of uncertainty of measurement of average temperature values for the cable with and without insulation. In addition, the uncertainty for the measured RMS current was determined using the following equation.

$$I_{RMS} = \sqrt{\frac{\bar{T}}{R_{th}R}} \tag{15}$$

In consequence the expanded uncertainty $U_{T(RMS)}$ for the RMS current is given as:

$$U_{T(RMS)} = \frac{\partial I_{RMS}}{\partial T} U_T = \frac{1}{2\sqrt{\bar{T}R_{th}R}} U_T \tag{16}$$

For I_{RMS}=4.6 A, mean temperature of the cable's core is about 43°C. For steel cable of L=1 m length, the thermal resistance is R_{th} = 14.5 K/W (Fig. 3). It denotes that $\partial I_{RMS}/\partial T \approx 0.073$ A/K and for I_{RMS}=4.6 A, the total expanded uncertainty is equal to $U_{T(RMS)}$=±0.18 A.

The comparison of the measurement uncertainty for average values of temperature and RMS current value allows concluding that using IR camera one can measure RMS current at high accuracy. It is a result of high temperature difference between the tested object and environment and registration and temperature averaging of relatively long sequence of images. One should notice that uncertainty of emissivity and ambient temperature was neglected. The cable and the insulation were covered by highly emission paint and ambient temperature was measured by high quality meter.

Tab. 4. Uncertainties of measured mean temperature registered by IR camera and RMS current for the cable with and without insulation for different current values

I_{RMS}	$T_{insulation}$	T_{core}
4.59 ± 0.18 A	39.38 ± 1.74°C	43.44 ± 1.85°C
5.45 ± 0.18 A	48.75 ± 1.99°C	55.2 ± 2.17°C
6.66 ± 0.13 A	60.48 ± 2.35°C	68.81 ± 1.69°C

5. Conclusions

Actual methods of measuring the RMS current value require proper selection of measuring equipment. Most of the methods need contact with the tested objects that are often under high voltage. The use of an IR camera allows contactless temperature measurement. The analysis of the recorded signal with knowledge of heat exchange coefficient, thermal parameters of the cable and insulation allow measurement of the RMS current value. The measured value agrees with results of thermal modeling using analytical approach. It leads to the conclusion, that RMS current can be measured with acceptable accuracy using IR thermography. During this research, one noticed 100 Hz harmonic of temperature spectrum in the registered sequence of the thermal images. In the next step research, the authors plan to measure this harmonic and verify its dependence from the RMS current and power dissipated in the cable. The first measurements have already been done and are very promising.

6. References

[1] IEC 60287-2-1:2015 RLV: Electric cables – Calculation of the current rating – Part 2-1: Thermal resistance – Calculation of thermal resistance. 2015.

[2] IEEE 738-2012: Standard for calculating the current-temperature relationship of bare overhead conductors. 2013.

[3] IEC 60287-2-3:2017: Electric cables - Calculation of the current rating - Part 2-3: Thermal resistance - Cables installed in ventilated tunnels, 2017.

[4] Morgan V.: External thermal resistance of aerial bundled cables. IEE Proceedings C, vol. 140, no. 2, pp. 65-72, 1993.

[5] Slaninka P.: External thermal resistance of air-installed power cables. Proceedings of IEE, vol. 116, no. 9, pp. 1547-1552, 1969.

[6] Whitehead S., Hutchings E.E.: Current rating of cables for transmission and distribution. Journal of the Institution of Electrical Engineers, vol. 83, no. 152, pp. 517-557, 1938.

[7] Theodosoglou I., Chatzipanagiotou P., Chatziathanasiou V., Boier A., Rata M.: Measurement and calculation of thermal characteristics of an overhead power line. Acta Electrotech. Proc. 5th Int. Conf. Mod. Power. Syst., pp 474-478, 2013.

[8] Anders G.: Rating of electric power cables in unfavorable thermal environment. Wiley-IEEE Press, 2005.

[9] Chatziathanasiou V., Chatzipanagiotou P., Papagiannopoulos I., De Mey G., Wiecek B.: Dynamic thermal analysis of underground medium power cables using thermal impedance, time constant distribution and structure function. Appl. Therm. Eng., vol. 60, no. 1-2, pp. 256–260, 2013.

[10] Chatzipanagiotou P., Chatziathanasiou V., De Mey G., Wiecek B.: Influence of soil humidity on the thermal impedance, time constant and structure function of underground cables: A laboratory experiment. Appl. Therm. Eng., vol. 113, pp. 1444–1451, 2017.

[11] Neher J. H., McGrath M. H.: The calculation of the temperature rise and load capability of cable systems. AIEE, vol. 76, no. 3, pp. 752-764, 1957.

[12] Bergman T., Lavine A., Incropera F., DeWitt D.: Introduction to Heat Transfer. John Wiley & Sons, Inc., 2011.

[13] Brito Filho J.P.: Heat transfer in bare and insulated electrical wires with linear temperature-dependent resistivity. Applied Thermal Engineering, vol. 112, pp. 881–887, 2017.

[14] Sedaghat A., de León F.: Thermal Analysis of Power Cables in Free Air: Evaluation and Improvement of the IEC Standard Ampacity Calculations. IEEE transactions on power delivery, vol. 29, no. 5, pp. 2306–2314, 2014.

[15] Koszmider A., Olak J, Piotrowski Z.: Przekładniki prądowe, WNT, Warszawa 1985.

[16] Więcek B., Pacholski K., Olbrycht R., Strąkowski R., Kałuża M., Borecki M., Wittchen W.: Termografia i spektrometria w podczerwieni, Zastosowania przemysłowe, Warszawa 2017.

[17] Więcek B., De Mey G.: Termowizja w podczerwieni podstawy i zastosowania, Wyd. PAK, Warszawa 2011.

[18] Theodosoglou I., Chatziathanasiou V., Papagiannakis A., Więcek B., De Mey G.: Electrothermal analysis and temperature fluctuations prediction of overhead power lines, Electrical Power and Energy Systems 87 (2017) 198-210.

[19] Wiecek B., De Mey G., Chatziathanasiou V., Papagiannakis A., Theodosoglou I.: Harmonic analysis of dynamic thermal problems in high voltage overhead transmission lines and buried cables. Electrical Power and Energy Systems 58 (2014) 199-205.

[20] Kulik A.: Aspekty zastosowania światłowodowego pomiaru temperatury punktów gorących w wysokonapięciowych uzwojeniach transformatorów dużych mo. Przegląd Elektrotechniczny Nr 11/2017.

[21] De Oliveira A., De Oliveira J.C., Resende J.W., Miskulin M.S.: Practical approaches for AC system harmonic impedance measurements. IEEE Transactions on Power Delivery, vol 6, no. 4, pp. 1721-1726, 1991.

[22] Crescentini M., Marchesi M., Romani A., Tartagni M., Traverso P. A.: A Broadband, On-Chip Sensor Based on Hall Effect for Current Measurements in Smart Power Circuits. IEEE Trans. on Instr. and Meas. Vol. 67, no. 6, pp.1470-1485, 2018.

[23] Brodziński G., Listowiec A. Dzierżanowski W.: Przetworniki pola magnetycznego nowej generacji w zabezpieczeniach ziemnozwarciowych kopalnianych linii energetycznych.

[24] Miedziński B., Szymański A., Dzierzanowski W., Wojszczyk B.: Performance of Hall sensors when used in ground fault protections in MV networks, UPEC 2004.

Received: 09.03.2018 *Paper reviewed* *Accepted: 04.05.2018*

Błażej TORZYK, MSc

He received BSc degree in Electronics and Telecommunication at Technical University of Lodz in 2013 and the MSc degree in Electrical Engineering, specialization Electric Power Engineering in 2015. Currently he is a PhD student at the Electronic Circuits and Thermography Department of Lodz University of Technology. His research interests lie in the fields IR thermography at power electronics systems and devices.

e-mail: blazejt@gmail.com

Prof. Bogusław WIĘCEK

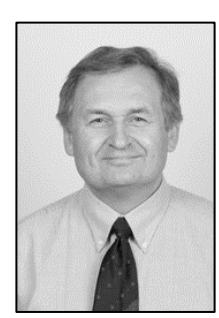

Bogusław Więcek is the head of Electronic Circuit and Thermography Division in Institute of Electronics where he has worked for more than 35 years. His scientific interests are: industrial and biomedical applications of IR thermography, heat transfer modelling and advanced IR analog and digital system developments. He is responsible for organizing the largest conference on thermography in Central and Eastern Europe every 2 years – Thermography and Thermometry Conference TTP.

e-mail: boguslaw.wiecek@p.lodz.pl